Dr. Mark Nansteel Molten Metal Plasma Cell Calorimetry: Data and Analysis (January, 2020)

Summary

Four molten metal calorimeter tests are analyzed and discussed in this document. The experiments were observed at BLP in Cranbury during the period 11/12/19-11/18/19. These tests featured four-inch cubical or six-inch spherical stainless-steel plasma cells, each incorporating an internal mass of liquid gallium or Galinstan which served as a molten metal bath for calorimetric determination of the power balance of BLP's proprietary hydrino plasma reaction maintained in its SunCell®. The molten metal also acted as cathode in formation and operation of the very-low voltage, high-current plasma while a tungsten electrode acted as the anode when electrical contact was made between the electrodes by electromagnetic pump injection of the molten metal from the cathode to anode. The plasma formation depended on the injection of either 2000 sccm H_2/20 sccm O_2 or 3000 sccm H_2/50 sccm O_2. This report includes description of the test apparatus and test procedure, a systematic development of the proper forms of energy conservation to be applied in the calorimetric measurement, modeling and analysis of the heat losses in the tests, and analysis of the thermal and electrical data to obtain the calorimetric measurement of plasma energy release. The excess powers in the range of 60 kW to over 200 kW with gains in the range of 2 to 3 times the power to maintain the hydrogen plasma reactions are given in the Tables of Appendix 3 at the end of this document and Table S1 *infra*. There was no chemical change observed in cell components as determined by energy dispersive X-ray spectroscopy (EDS). The power from the combustion of the H_2/ 1%O_2 fuel and HOH catalyst source was negligible (16.5 W for 50 sccm O_2 flow) and occurred outside of the cell. Thus, the theoretical maximum excess power from conventional chemistry was zero.

Analysis Methods

The four tests are denoted by

MM1: (10/15/19) 6-inch spherical cell (Galinstan-fill); no liner; DC rectifier electrode power
MM2: (11/15/19) 4-inch cubical cell (gallium-fill); 2 mm tantalum liner; DC capacitor electrode power
MM3: (11/13/19) 4-inch cubical cell (gallium-fill); 3 mm tungsten liner; DC rectifier electrode power
MM4: (11/13/19) 4-inch cubical cell (gallium-fill); 3 mm tungsten liner; DC rectifier electrode power

In these tests plasma energy release was determined from measurements of electrical energy input and system enthalpy rise as well as an estimate of the heat lost to the surroundings:

$$E_{Plasma} = (\text{System enthalpy rise} - \text{Electrical energy input}) + \text{Heat loss} \qquad (S1)$$

The enthalpy rise and energy input are obtained from straightforward temperature, voltage and current measurements. The system temperature was characterized by measurements at only two positions in the cell, however, modeling suggests that during quasi-equilibrium cool-down the cell is approximately isothermal. Therefore, the temperature measurement at just two points is probably sufficient. Also, detailed examination of the electrical power input data suggests that the 5 or 10 kHz rate used to sample the data is more than adequate to resolve the observed power fluctuations. Hence, the enthalpy rise and energy input terms in (S1) are determined with satisfactory precision. However, the heat loss can only be estimated. The method of estimation developed and applied in the present report is consistent with basic heat transfer principles.

In all four test cases strong plasma energy release was observed. In each case the plasma energy was greater than the electrical energy input to the system. Therefore, the gain

$$\eta = \frac{\text{Plasma energy} + \text{Electric input}}{\text{Electric input}}$$

always exceeded two. In one case the gain exceeded three, implying that the plasma energy was more than twice the electric input energy. The plasma energy, power and gain measured in the four tests are tabulated in Table S1. Following termination of each plasma run, very conservative thermal equilibration durations were implemented here in order to ensure that adequate time expired for the cell to reach isothermal, quasi-equilibrium cool-down conditions. There is no net energy effect of this if losses are accounted for exactly, but unfortunately these can only be estimated. Note, however, that complete disregard of the (uncertain) energy loss still results in plasma energy gains exceeding two, cf. *Test Results.*

Table S1. Calorimetric Energy, Power, and Gain Measurements

	Present		
	E_{Plasma} [kJ]	Excess Power P_{Plasma} [kW]	η [1]
MM1	1693	75.6	3.19
MM2	272.9	215	2.28
MM3	930.5	77.6	2.49
MM4	1425	82.4	2.67

Molten Metal Calorimeter System and Measurement Method

System Description

The molten metal calorimeter arrangement is shown schematically in Fig. 1A and photographically in Figs. 1B and 1C. The plasma cell may be of cubic shape, as depicted in Fig. 1, or it may be spherical. In the case of a cubical cell the 347 stainless steel plasma cell body is an edge-welded cube, 4 inches on a side. A circular opening in the top wall of the cube is welded to a cylindrical transition section which is, in turn, welded to a circular ConFlat vacuum flange. A matching blank ConFlat flange incorporating an electrically isolated feed-through having a penetrating copper bus bar is bolted to the ConFlat vacuum flange with a silver-plated gasket to create a vacuum seal. Inside of the cell, the copper bus bar is welded to a solid tungsten bus bas and a 1.2 kg solid tungsten cylinder electrode with a concave end. The bus bars where covered by a boron nitride (BN) insulator attached by compression from the larger diameter tungsten electrode that is screwed onto the tungsten bus bar. The cubical cell is typically filled with about 2.5 kg of liquid gallium.

During operation the gallium is circulated in the cell by the electromagnetic pump (EMP) which is located just below the cell body and is connected to it by a U-shaped stainless steel tube. The cell walls are 0.25 inch thick and the vertical walls are lined on the inside with tungsten or tantalum plates, with about 3 mm or 2 mm thickness, respectively, in order to prevent alloying of the gallium with various components of the stainless steel. The absence of any alloy formation or the formation of any gallium oxide was shown by energy dispersive X-ray spectroscopy (EDS) analysis result of 100% Ga following the runs. The spherical plasma cell similarly incorporates the upper ConFlat flange with electrode and the EMP below the cell body. The 6-inch diameter spherical cell is also 347 stainless steel with 0.25 inch wall thickness. The spherical cell features no liner and is filled with about 3.4 kg of liquid Galinstan. Each cell,

cubic or spherical, is supplied a steady hydrogen-rich stream of hydrogen and H_2O gas formed by the recombination of $H_2/1\%O_2$ external to the cell by a 10% Pt/Al_2O_3 catalyst. This mixture is evacuated following reaction in the cell under flow conditions. The dynamic flow and pumping results in a steady-state pressure of a few Torr. Not shown in Fig. 1 are the 2 inch diameter multi-strand copper power cables that connect to the upper and lower cell electrodes, the two K-type thermocouples that measure the cell internal temperature, and various supporting connections and structure.

During operation the EMP is powered by a current-controlled DC power supply (Matsuda Precision REK10-1200); whereas, the cell electrodes are powered either by a switch-mode rectifier or by discharging a bank of capacitors. Specifically, the constant ignition current of 1500 A is supplied by a LabVIEW-controlled (National Instruments) switch-mode rectifier (Model: American CRS Q500 IP32) rated to a maximum of 50V/1500A. The ignition current of about 3000 A is supplied by a capacitor bank comprised 3 parallel banks of 18 capacitors (Maxwell Technologies K2 Ultracapacitor 2.85V/3400F) in series that provided a total bank voltage capability of 51.3V with a total bank capacitance of 566.7 Farads that was initially charged to 50 V. The cell electrodes are connected to either power source such that the tungsten electrode is the anode (negative) and the liquid metal (gallium for cubic cells and Galinstan for the spherical cell) is the cathode (positive). Electrode voltage and current are monitored and recorded by a high-sample-rate, high-resolution oscilloscope (PicoScope 5000 Series) using a voltage differential probe (PicoTech TA041, ±70V) and a DC Hall effect current probe (GMW CPCO-4000-77-BP10, ±4 kA).

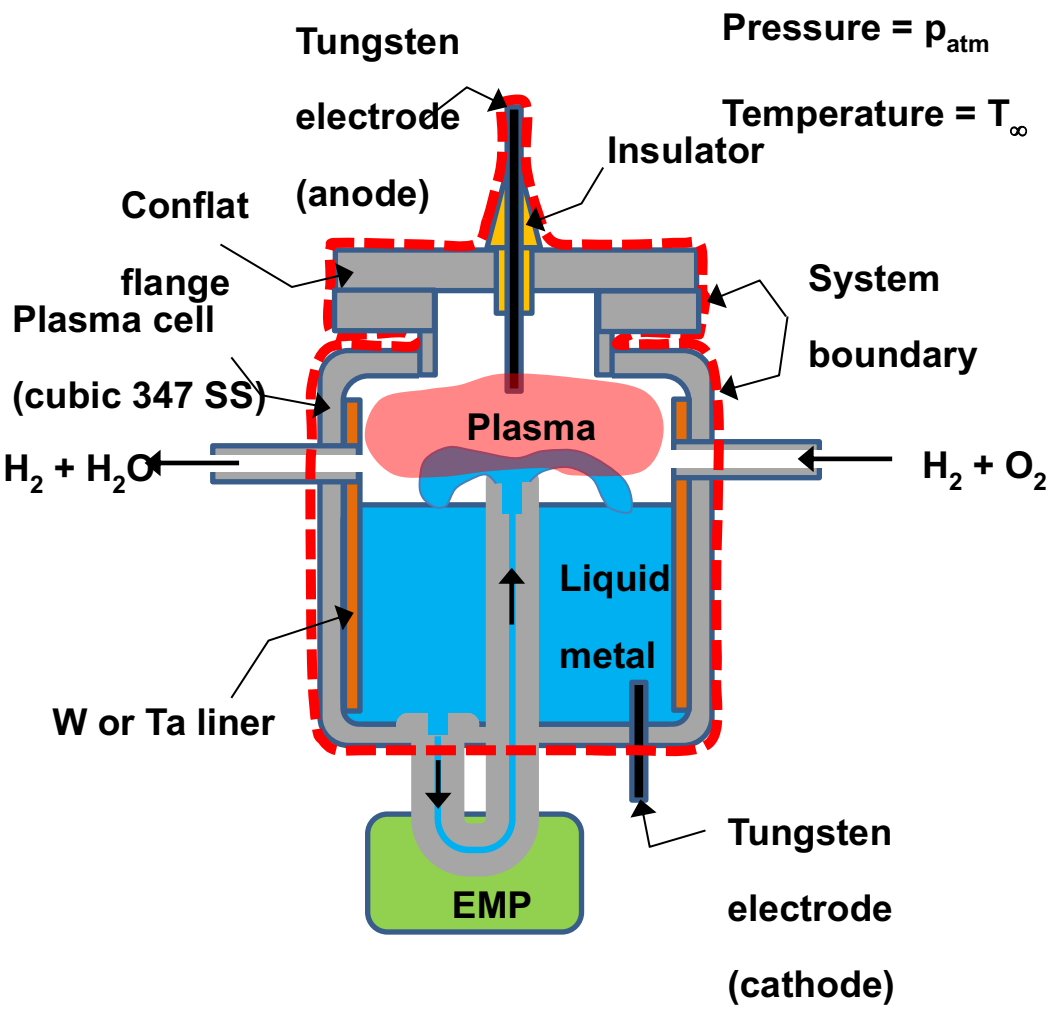

Figure 1A. Plasma Cell Schematic

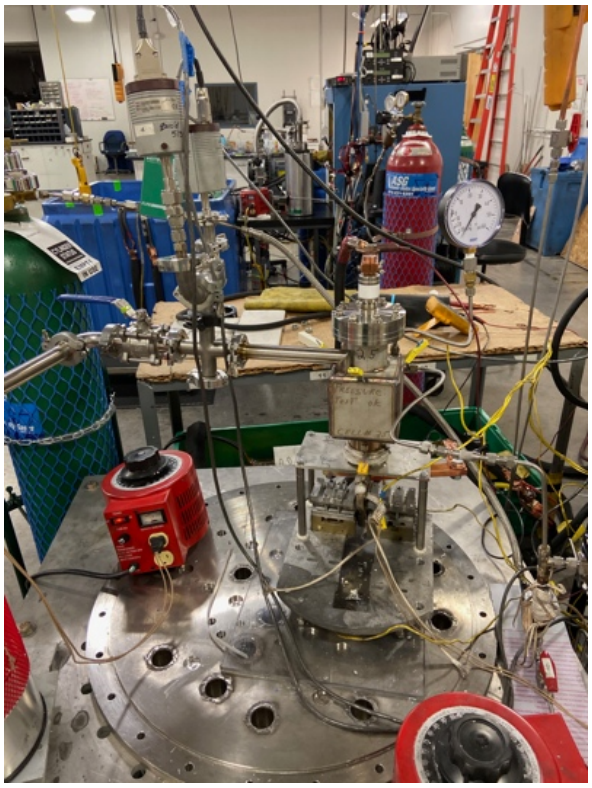

Figure 1B. Photograph of SunCell® and Molten Metal Calorimeter System

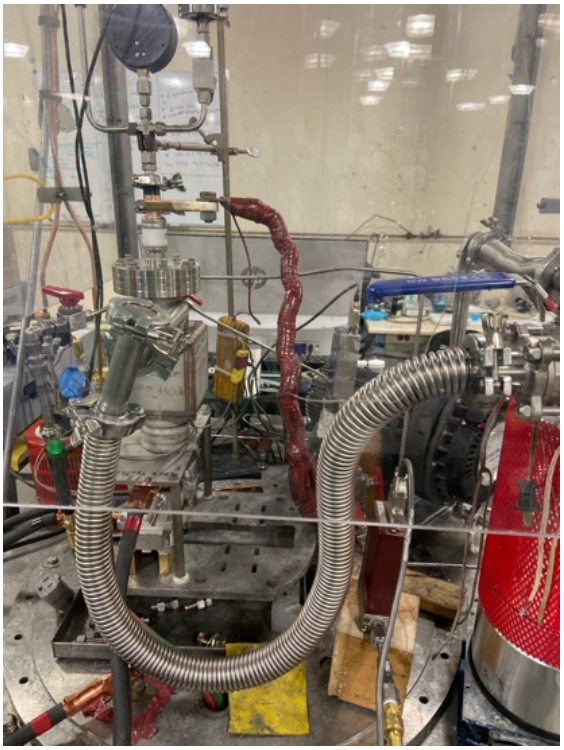

Figure 1C. Photograph of SunCell® and Molten Metal Calorimeter System

Calorimetric Test Procedure

The cell is filled with a known mass of liquid metal, then sealed and evacuated to ~15 mTorr pressure. The hydrogen/oxygen flow is started and maintained constant by two mass flow controllers such that between about 2000 and 3000 sccm of H_2 99%/1% O_2 mixture flows into an external 10% Pt/Al_2O_3 recombiner, and the resulting H_2 gas with 1% H_2O gas flows into the cell under dynamic vacuum at an operating pressure of a few Torr. The various parts of the system at this time are all at the uniform temperature T_1. Then, power is simultaneously applied to the cell electrodes and the EMP. This time is the start of the calorimetric test and is denoted as time t_1. Power supply to the EMP and the electrodes results in liquid metal circulation and plasma formation in the cell, cf. Figs. 1A-C. During the test, plasma conditions in the cell are monitored by observing the electrode voltage and current as well as the cell temperature as indicated by the two internal liquid metal-immersed thermocouples. The cell exterior surface is also carefully observed during the run, in order to identify localized areas of intense heating by the plasma. These so-called "hot-spots" are recognized by local surface incandescence. If these occur the test run is terminated to prevent cell damage or destruction. Otherwise, at time t′ power to the cell electrodes is terminated, extinguishing the plasma, while power to the EMP is maintained. Continuing to power the EMP for several minutes after powering off the cell electrodes promotes mixing of the liquid metal in the cell, facilitating a faster approach to a quasi-equilibrium cool-down condition. This condition is indicated by convergence of the two internal cell thermocouple responses. When the cell thermocouples are judged to have converged sufficiently, power to the EMP is also terminated. This is the end of the test, which corresponds to time t_2 and uniform cell temperature T_2.

During the test run, voltage and current at the cell electrodes are sampled every 0.2 or 0.1 ms corresponding to 5 or 10 kHz sampling rates, respectively. The corresponding energy supply to the electrodes is determined by trapezoidal integration of the power, which is taken as the product of the sampled voltage and current during the time interval $t_1 \le t \le t'$. The cell temperature, indicated by the two K-type internal thermocouples, is acquired once every second. The rate of heat loss from the cell to the surroundings is not measured.

Energy Conservation

The net enthalpy external to the cell due to the hydrogen/oxygen gas reaction has been shown to be less than about 20 W, the gas recombination occurs outside of the cell, and the temperature difference between the liquid metal inlet and exit streams is small. Therefore, the small energetic contributions due to these through-flows are ignored, and so for the purpose of energy conservation the plasma cell is considered a closed thermodynamic system, cf. Fig. 1. Energy conservation for this system (under constant pressure p_{atm}), in rate form, requires

$$P_{Elect} + P_{Plasma} - \dot{Q}_{Loss} = \frac{dH}{dt} \qquad (1)$$

where the system enthalpy is denoted by H and $\dot{Q}_{Loss}$ is the rate of heat loss from the cell due to radiation and convection to the environment as well as losses by conduction to the

electromagnetic pump, support structure, electrical cables, etc. The electrode power input and plasma power generation rates are denoted by P_{Elect} and P_{Plasma}, respectively. It is shown in Appendix 1 that the time rate of system enthalpy change on the right of (1) can be expressed in terms of products of the mass-weighted average specific heat and time derivatives of the mass-weighted average temperature for the various sub-parts of the cell, e.g. liquid metal, stainless cell body, tungsten or tantalum liner, and stainless, tungsten or boron nitride electrode parts, etc.:

$$P_{Elect} + P_{Plasma} - \dot{Q}_{Loss} = \sum m_i C'_{pi} \frac{dT'_i}{dt} \qquad (2)$$

Equation (2) allows for non-isothermal behavior of the various sub-parts of the system such that primed quantities are spatially averaged over the mass of component part i but are time dependent. Integrating (2) from start time t_1 to the end time t_2 yields

$$E_{Elect} + E_{Plasma} - Q_{Loss} = \left(\sum m_i C_{pi}\right)(T_2 - T_1) \qquad (3)$$

where the energies on the left are

$$E_{Elect} = \int_{t_1}^{t'} P_{Elect}\,dt, \quad E_{Plasma} = \int_{t_1}^{t'} P_{Plasma}\,dt, \quad Q_{Loss} = \int_{t_1}^{t_2} \dot{Q}_{Loss}\,dt$$

and C_{pi} is the specific heat of component i averaged over temperatures ranging from the initial temperature T_1 to the final temperature T_2. Here, isothermality ($T_i = T_2$) of the various cell parts at time t_2 has been assumed, cf. Appendix 1. The plasma energy can be calculated from (3) using measurements of the system temperature change and the electrode input energy, provided that some estimate of the heat loss is available. Also note from (3) that a change in system enthalpy rise due to a change in the final temperature T_2, by extending or contracting the run termination time t_2, must be exactly balanced by a change in heat loss of the same magnitude but opposite sign.

Heat Loss: General Discussion and Modeling Estimates

Heat loss from the cell occurs by conduction, convection and radiation to the environment. The rate of heat loss is mostly a function of the cell surface temperature, which is shown below to deviate only modestly from the mean cell temperature, except perhaps during the rapid heat-up phase of the calorimetric run, $t < t'$. During the heat up the surface temperature is lower than the mean cell temperature, which tends to reduce the heat loss. But this effect is mitigated by transient conduction and convection effects which enhance the heat transfer during this period for a given surface temperature. Because of these mitigating effects it is assumed that the instantaneous rate of heat loss from the cell depends only on the cell temperature as measured by the two internal thermocouples. This assumption, which is an approximation, allows for a rational estimate of heat loss in a later section. Assuming the environment temperature to be T_∞, the heat loss rate and the total loss are

$$\dot{Q}_{Loss} = f(T_{Cell} - T_\infty), \qquad Q_{Loss} = \int_{t_1}^{t_2} f(T_{Cell} - T_\infty)\,dt$$

where f is a positive, increasing function of its argument. This functional relation includes heat loss by conduction and convection, $\propto (T_{Cell} - T_\infty)$, and nonlinear convection effects, $\propto (T_{Cell} - T_\infty)^\gamma$, as well as radiative loss effects, $\propto (T_{Cell}^4 - T_\infty^4) \propto g(T_{Cell} - T_\infty)$. Clearly, Q_{Loss} depends on the cell temperature history during the test, which encompasses both the temperature levels experienced by the cell and the time elapsed at elevated temperature.

The most obvious heat losses occur from the cell wall external surface. These losses occur by conduction through the cell wall from the hot liquid metal and then by free convection and radiation from the cell external surface to the environment. The process is shown schematically in Fig. 2 for the vertical wall of a cubical cell with a liner of thickness δ_{Liner}. Ignoring transient effects, the surface temperature T_S is sufficiently large that steady conduction through the wall is balanced by steady convection and radiation from the surface. The rate of free convection from the surface of an isothermal cube is given by the correlations of Yovanovitch and Jarfarpur [1]. The heat transfer process is similar for a spherical cell, which operates without a liner. The procedure for calculating the cell surface temperature and the rates of convection and radiation loss is given in Appendix 2. Table 1 shows the estimated cell surface temperature, heat fluxes (W/m^2) and heat loss rates for liquid metal temperatures T_{LM} = 400, 500, and 600°C. These results assume a stably oxidized 347 stainless steel exterior surface ($\varepsilon \sim 0.88$). It is important to note that the temperature drop through the cell wall is no greater than about 11°C. The total surface heat flux is similar for the 4-inch cube cell and the 6-inch spherical cell, amounting to about 32 kW/m^2 for 600°C liquid metal temperature. Also, the rate of heat loss by radiation is about 77% of the total heat loss for a 400°C liquid metal temperature, increasing to about 86% for T_{LM} = 600°C.

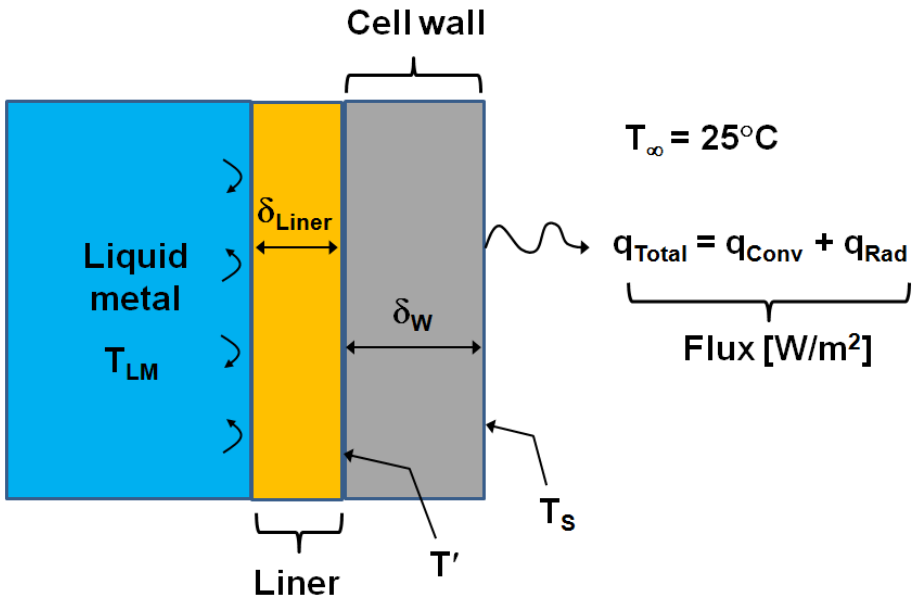

Figure 2. Heat Flow Through Cell Wall (Schematic)

For the 4-inch cubical cell, considering the nominal surface area of 619 cm^2, the surface heat loss rate by convection and radiation is about 0.77, 1.3 and 2.0 kW for liquid metal temperatures of 400, 500 and 600°C, respectively, cf. Table 1. These estimates are certainly low since they ignore the considerably enhanced surface area of the actual cell owing to the large upper vacuum flange and electrode assembly and the observation that the Ta liner having a melting point of 3017 °C was observed to melt in some runs. Even greater losses from the cell are expected to occur by conduction through the large copper cables which connect to the cell electrodes. These two multi-strand cables, each with 2-inch nominal diameter, are responsible for steady losses of about 2.3, 2.9 and 3.5 kW for cell temperatures of 400, 500 and 600°C, ignoring strand packing efficiency and assuming a conduction length of 25 cm, cf. Table 2. These cable loss estimates also represent lower bounds since transient and convection effects have been ignored. Moreover, the tungsten anode and cell liner have been observed to melt during operation indicating that the corresponding temperature exceeds the melting point of tungsten (M.P. = 3422 °C) such that the corresponding losses may be highly underestimated. Additional conduction losses from the cell also occur due to the various other connections to the cell, e.g. conduction loss to the EMP through the liquid metal-filled stainless connecting tube and the metal cell support structure. Hence, it is expected that total losses from the cell may exceed 5 kW for a cell temperature of 400°C.

Table 1. Cell Wall Surface Temperature and Heat Transfer Rates

	T_{LM} [°C]	T_S [°C]	q_{Conv} [W/m^2]	q_{Rad} [W/m^2]	q_{Total} [W/m^2]	$q_{Total}A$ [kW]
4-inch 347 SS cube 3 mm tungsten liner	400	395.8	2793	9596	12,389	0.767
	500	493.1	3622	16,802	20,424	1.27
	600	589.2	4476	27,201	31,677	1.96
6-inch 347 SS sphere no liner	400	396.1	2833	9612	12,445	0.910
	500	493.5	3674	16,842	20,516	1.50
	600	589.9	4540	27,289	31,829	2.32

Table 2. Conduction Loss Through the Copper Connection Cables

Cell Temperature	Heat loss
400°C	2.3 kW
500°C	2.9 kW
600°C	3.5 kW

Heat Loss Estimate Based on Cell Temperature History

Actual heat loss rates from the system can be estimated using cell temperature vs. time data for times $t > t'$ during which there is no electrode power supply or plasma power generation. During this cool-down phase the cell is mostly isothermal, so using energy conservation (2) and ignoring small differences in temperature between the cell parts yields

$$\dot{Q}_{Loss} = -\left(\sum m_i C_{pi}\right)\frac{dT_{Cell}}{dt} \qquad (4)$$

Equation (4) and numerical differentiation of the cell temperature data results in a rough estimate for the rate $\dot{Q}_{Loss}$ as a function of cell temperature. Using selected data from the cool-down phase in tests MM3 and MM4, and data from the cool-down in the low-temperature calibration test, some loss rates from (4) are plotted versus the cell temperature in Fig. 4. Data were selected from the quasi-equilibrium cooling phase, well after cessation of electrode power and plasma power generation. These three data sets were selected in order to span a broad range of cell temperature. The highly approximate nature of this approach is emphasized by the very large scatter in the $\dot{Q}_{Loss}$ data, especially for test MM3. In any case, the data exhibit the correct trend of increasing heat loss rate with temperature as well as upward concavity corresponding to increasing radiation loss. Also note that these data suggest a loss rate of about 6 kW for a 400°C cell temperature, as suggested by the rough modeling calculations above. Also appearing in Fig. 4 is the best-fit curve of the form

$$\dot{Q}_{Loss} = A(T_{Cell} - T_\infty) + B(T_{Cell}^4 - T_\infty^4) \qquad (5)$$

which includes the expected linear dependence of the losses for conduction and convection effects as well as the quartic dependence for the radiation loss. The temperature of the surroundings in the fit was selected as $T_\infty = 25°C = 298.15$ K. This function provides a simple, though very approximate, means for estimating the loss rate from the cubical cell at a given temperature. Although the fit is based on data for cube cells, at this crude level of approximation it may be used to estimate losses from the spherical cell as well. The approximate loss rate (5) is used to estimate the lost energy in each test run according to

$$Q_{Loss} = \int_{t_1}^{t_2} \dot{Q}_{Loss}(T_{Cell})dt$$

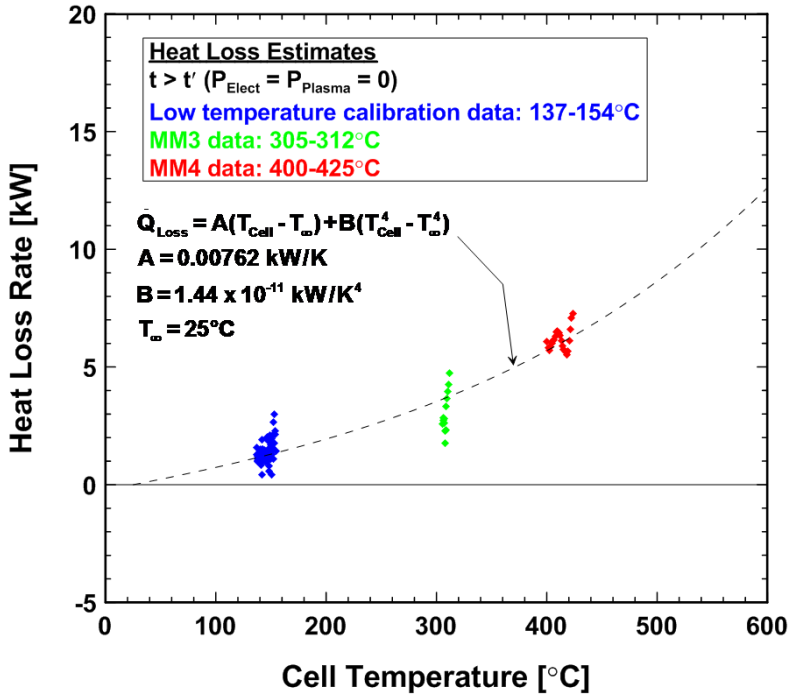

Figure 4. Cell Heat Loss Rate as a Function of Cell Temperature

Test Results

Results of four calorimetric tests are analyzed and discussed here:

MM1: (10/15/19) 6-inch spherical cell (Galinstan); no liner; DC rectifier electrode power
MM2: (11/15/19) 4-inch cube cell (gallium); 2 mm tantalum liner; DC capacitor electrode power
MM3: (11/13/19) 4-inch cube cell (gallium); 3 mm tungsten liner; DC rectifier electrode power
MM4: (11/13/19) 4-inch cube cell (gallium); 3 mm tungsten liner; DC rectifier electrode power

Test MM1

This test used the 6-inch un-lined spherical stainless cell filled with 3.4 kg of liquid Galinstan. DC electrode power was supplied by the American CRS switch mode rectifier for 22.43 s as shown in Fig. 5. Although voltage fluctuated throughout this time the mean voltage rose gradually to about 35 V by the end of the period and current, also fluctuating, averaged near 1.2 kA. The power averaged near 40 kW toward the end of the power addition period. Figure 6 shows that the 5 kHz sampling rate was large enough to adequately resolve the fluctuations in voltage and current. Trapezoidal integration of the power resulted in the electrode energy input E_{Elect} = 775 kJ.

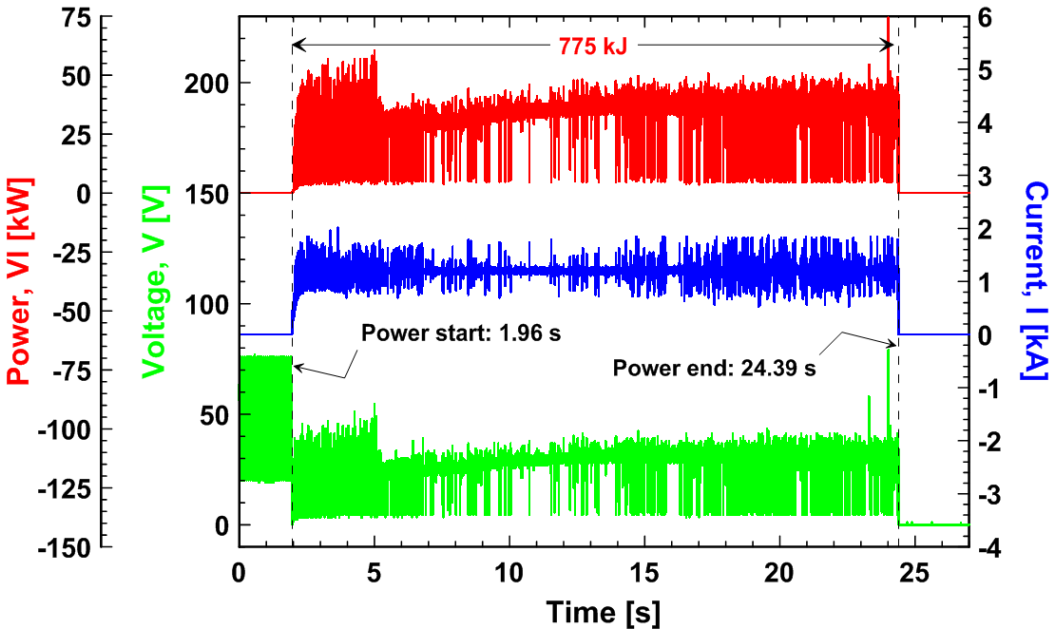

Figure 5. VI Data in Test MM1

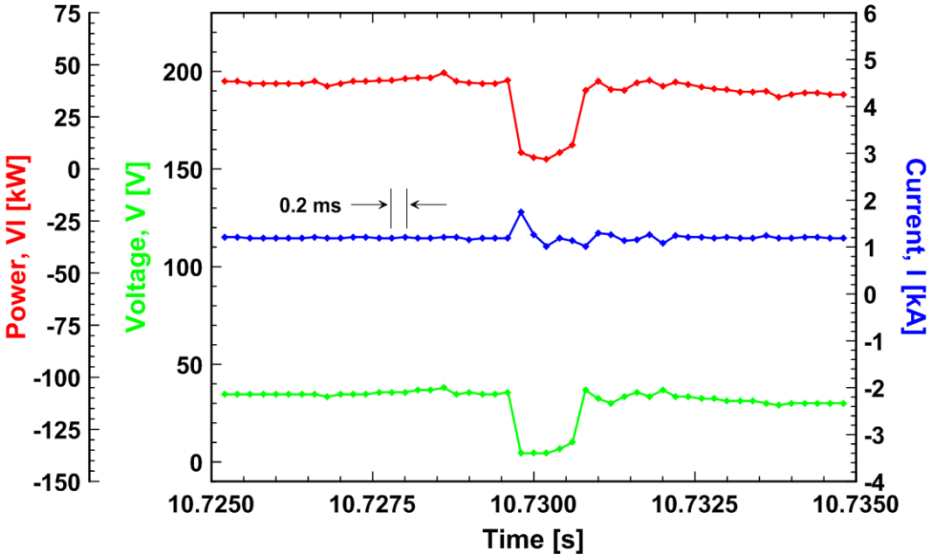

Figure 6. VI Data with Expanded Time Scale in Test MM1

The two measured cell temperatures and the average temperature are plotted vs. time in Fig. 7. By careful observation of the cell temperature response the start time for the test was determined to be t_1 = 77 s at which time the cell temperature was T_1 = 87.7°C. Power input is terminated 22.43 s later at t′ = 99.43 s. During this period the cell temperature rises rapidly from about 88°C to about 620°C due to plasma power generation and electrode power input. When the electrode power is removed the cell temperature decays as the cell releases thermal energy to the

surroundings by conduction, convection and radiation. At time t_2 = 129 s the final cell temperature is T_2 = 477°C. At this time, the uncertainty in cell temperature (indicated by the difference in temperature for the two internal thermocouples) is less than 8°C, which is only slightly greater than 2% of the cell temperature change $T_2 - T_1$ = 389°C. The enthalpy rise of the cell during the run is $\Sigma m_i C_{pi} (T_2 - T_1)$ = 2042.5 kJ. Heat loss from the cell determined by the $\int \dot{Q}_{Loss}$-method is Q_{Loss} = 425.6 kJ. The large losses are due to the high mean cell temperature of about 451°C during the 52 s run. The corresponding hydrino reaction energy release and gain as well as the same parameters considering the extreme case of ignoring heat loss completely are:

$Q_{Loss} = 0$:	E_{Plasma} = 1268 kJ;	$\eta = 2.64$
$\int \dot{Q}_{Loss}$-method:	E_{Plasma} = 1693 kJ;	$\eta = 3.19$

The plasma energy is large enough compared to the electrode input energy that even when the losses are completely ignored the gain exceeds 2.5. The relative magnitudes of the various energy quantities in the energy balance are shown in the bar graph of Fig. 8. Of the three quantities that determine the plasma energy (Plasma energy = Enthalpy rise + Heat loss – Electrode energy) the enthalpy rise is the largest, followed by the electrode energy and the heat loss. All data used in the energy balances are tabulated in Appendix 3.

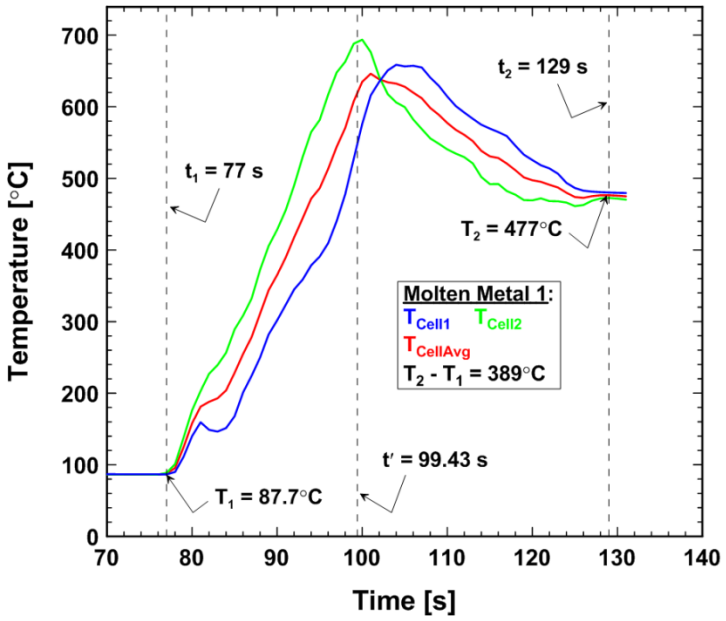

Figure 7. Cell Temperature Variations in Test MM1.

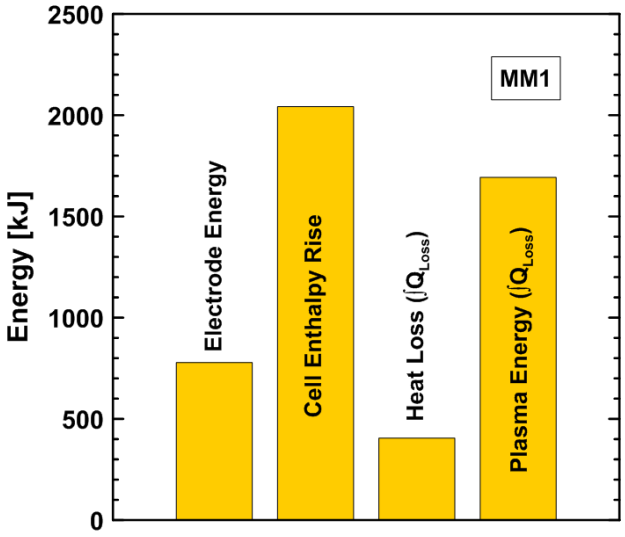

Figure 8. Energy Bar Graph for Test MM1.

Test MM2

This test used a 4-inch cube cell lined with 2 mm tantalum plates on the vertical interior cell walls. The cell was filled with 2.5 kg of liquid gallium. Electrode power was supplied by discharging a capacitor bank over a period of 1.27 s as shown in Fig. 9. Voltage was relatively steady, reducing from about 40 V to 35 V over the period. The current was mostly steady at about 4.5 kA except for some small fluctuations and the power was also mostly steady, averaging about 170 kW. Figure 10, with expanded time scale, shows that the 10 kHz sampling rate used in test MM2 was more than sufficient to adequately resolve the fluctuations in voltage and current. Trapezoidal integration of the power resulted in the electrode energy input E_{Elect} = 213 kJ.

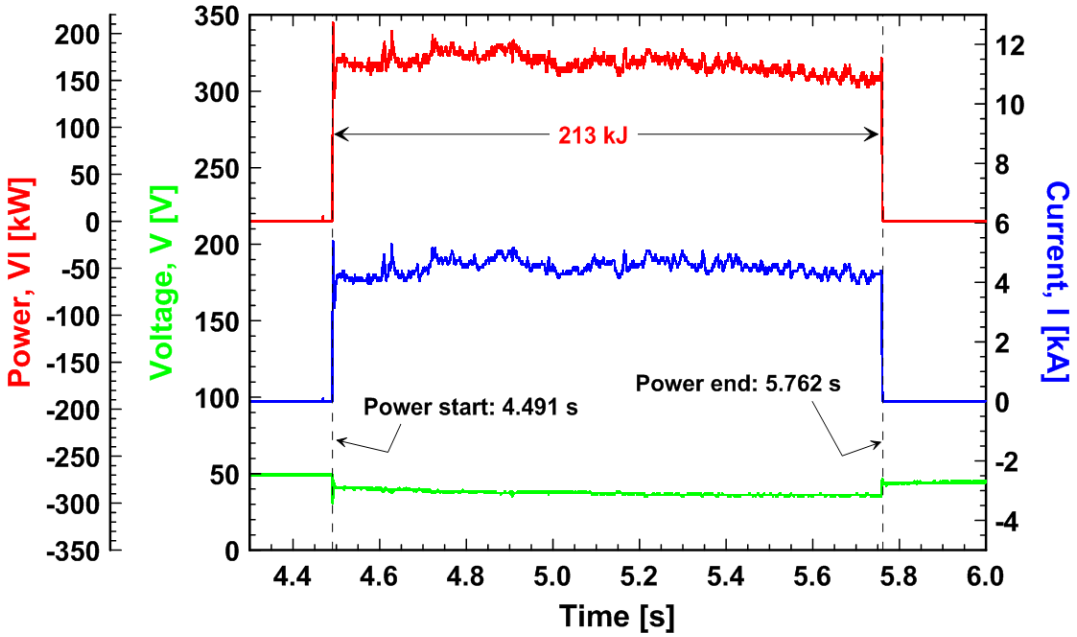

Figure 9. VI Data in Test MM2

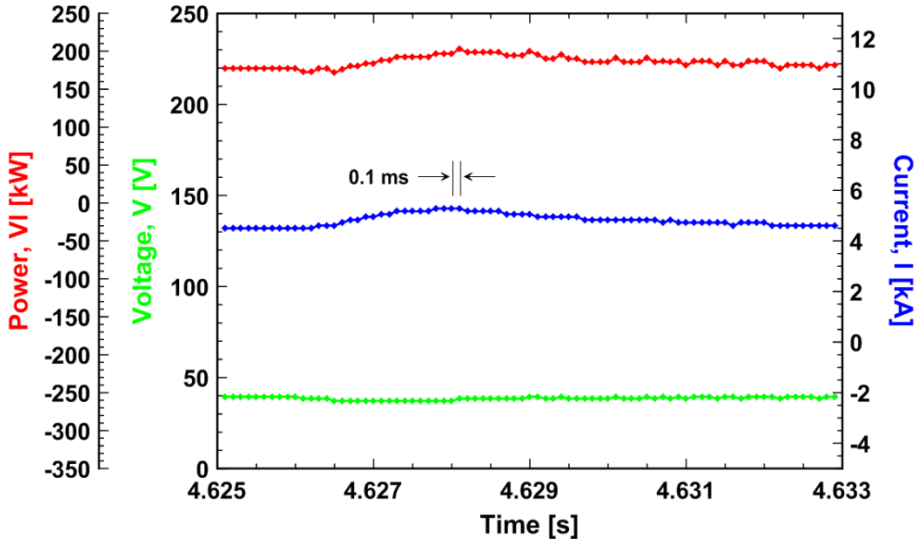

Figure 10. VI Data with Expanded Time Scale in Test MM2

The two cell temperatures and the average temperature are plotted vs. time in Fig. 11. The start time for the test was t_1 = 24 s at which time the cell temperature was T_1 = 56.3°C. Power input is terminated only 1.27 s later at t' = 25.27 s. During this brief period the cell temperature rises rapidly from about 56°C to about 85°C due to plasma power generation and electrode power input. When the electrode power is removed the cell temperature continues to rise for about an additional 4 seconds, ultimately reaching 155°C, before starting to decay due to heat loss to the surroundings. This behavior could be due to the deposition of a large amount of energy in a very

small localized volume inside the cell, which requires several seconds to spread over the cell and be sensed by the internal thermocouples. At time $t_2 = 50$ s the final cell temperature $T_2 = 138°C$. At this time the uncertainty in cell temperature (indicated by the difference in temperature for the two internal thermocouples) is about 2°C, which is only about 2.4% of the cell temperature change $T_2 - T_1 = 81.8°C$. The enthalpy rise of the cell is $\Sigma m_i C_{pi} (T_2 - T_1) = 455.9$ kJ. Heat loss by the $\int \dot{Q}_{Loss}$-method, $Q_{Loss} = 29.9$ kJ. The relatively small heat loss is due to the low average cell temperature, about 135°C, during the brief 26 s run time. The corresponding hydrino reaction energy release and gain as well as the same parameters considering the extreme case of ignoring heat loss completely are:

$Q_{Loss} = 0$:	$E_{Plasma} = 243.0$ kJ;	$\eta = 2.14$
$\int \dot{Q}_{Loss}$-method:	$E_{Plasma} = 272.9$ kJ;	$\eta = 2.28$

The relative magnitudes of the various energy quantities in the energy balance are shown in the bar graph of Fig. 12. The heat loss is again the smallest energy quantity. All data used in the energy balances are tabulated in Appendix 3.

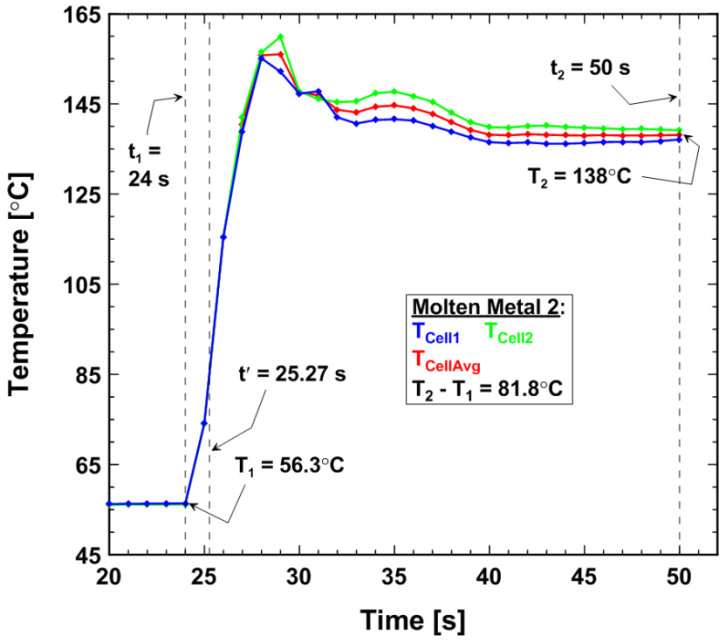

Figure 11. Cell Temperature Variations in Test MM2.

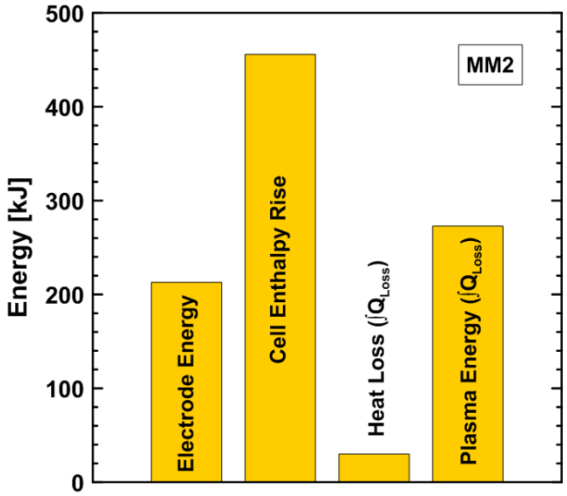

Figure 12. Energy Bar Graph for Test MM2.

Test MM3

This test used a 4-inch cube cell filled with 2.7 kg of liquid gallium and lined with 3 mm tungsten plates on the vertical interior cell walls. Electrode power was supplied by the American CRS switch mode rectifier over a period of 11.99 s as shown in Fig. 13. Voltage and current were sampled every 0.2 ms corresponding to a 5 kHz sampling rate. The voltage fluctuated around 30 V, the current was more stable near about 1.6 kA and the power was also stable near 50 kW. Trapezoidal integration of the power resulted in the electrode energy input E_{Elect} = 626 kJ.

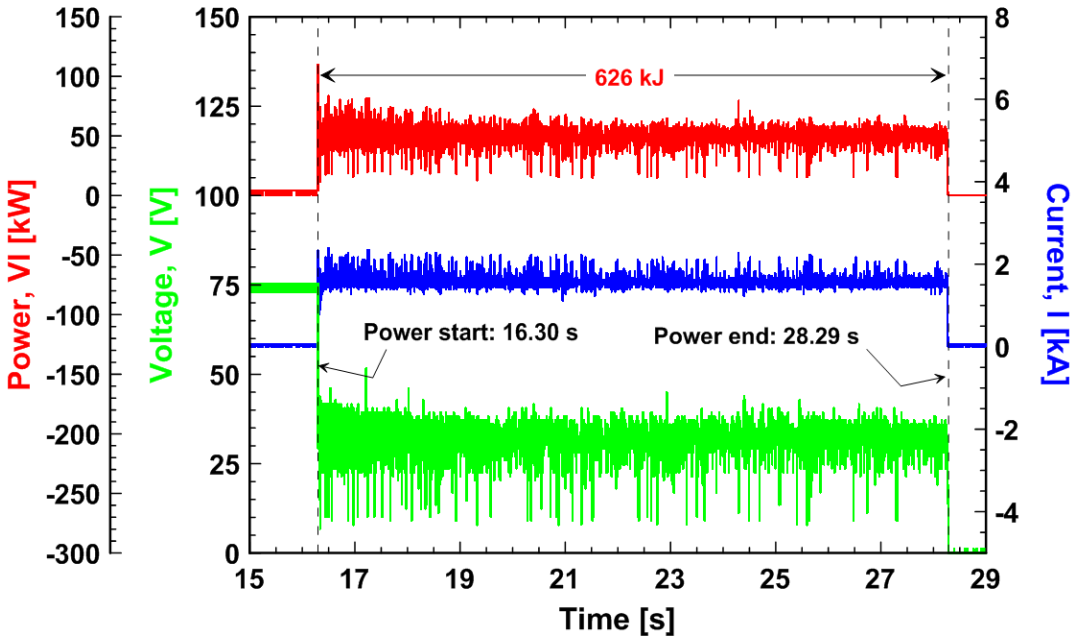

Figure 13. VI Data in Test MM3

The two cell temperatures and the average temperature are plotted vs. time in Fig. 14. The start time for the test was $t_1 = 111$ s at which time the cell temperature was $T_1 = 83.5$°C. Power input is terminated 11.99 s later at $t' = 122.99$ s. During this period the cell temperature rises rapidly from about 84°C to about 380°C due to plasma power generation and electrode power input. When the electrode power is removed the cell temperature decays in a mostly linear fashion due to heat loss to the surroundings. At time $t_2 = 155$ s the final cell temperature is $T_2 = 326$°C. At this time the uncertainty in cell temperature (indicated by the difference in temperature for the two internal thermocouples) is about 9.9°C, which is about 4% of the cell temperature change $T_2 - T_1 = 243$°C. The cell enthalpy rise is $\Sigma m_i C_{pi} (T_2 - T_1) = 1382.2$ kJ. Heat loss by the $\int \dot{Q}_{Loss}$-method, $Q_{Loss} = 174.0$ kJ. The corresponding hydrino reaction energy release and gain as well as the same parameters considering the extreme case of ignoring heat loss completely are:

$Q_{Loss} = 0$:	$E_{Plasma} = 756.5$ kJ;	$\eta = 2.21$
$\int \dot{Q}_{Loss}$-method:	$E_{Plasma} = 930.5$ kJ;	$\eta = 2.49$

The relative magnitudes of the various energy quantities in the energy balance are shown in the bar graph of Fig. 15. Note that in test MM3 the heat loss accounts for about 30% of the plasma energy, suggesting that a more careful analysis of loss effects is justified. All data used in the energy balances are tabulated in Appendix 3.

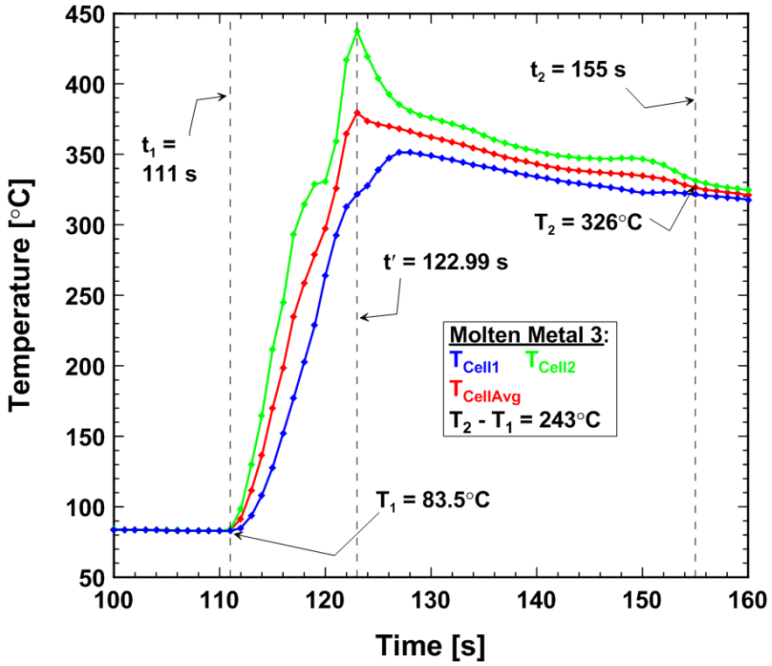

Figure 14. Cell Temperature Variations in Test MM3.

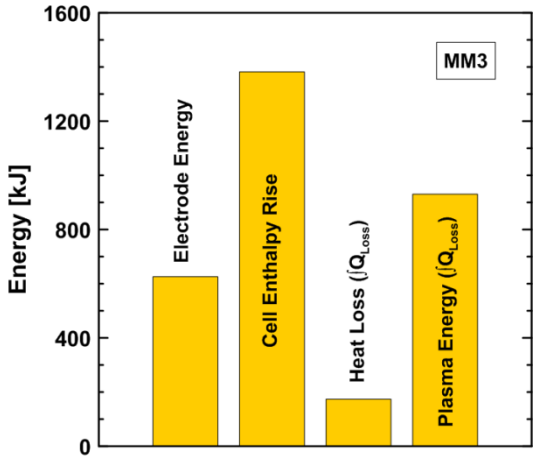

Figure 15. Energy Bar Graph for Test MM3.

Test MM4

Test MM4 used the same 4-inch cube cell lined with 3 mm tungsten plates and filled with 2.7 kg of liquid gallium as in test MM3. Electrode power was again supplied by the American CRS switch mode rectifier over a period of 17.3 s as shown in Fig. 16. Voltage and current were again sampled every 0.2 ms corresponding to a 5 kHz sampling rate. The voltage fluctuated around 30 V, the current was near 1.5 kA and the power was mostly stable near 50 kW. Trapezoidal integration of the power resulted in the electrode energy input E_{Elect} = 853 kJ.

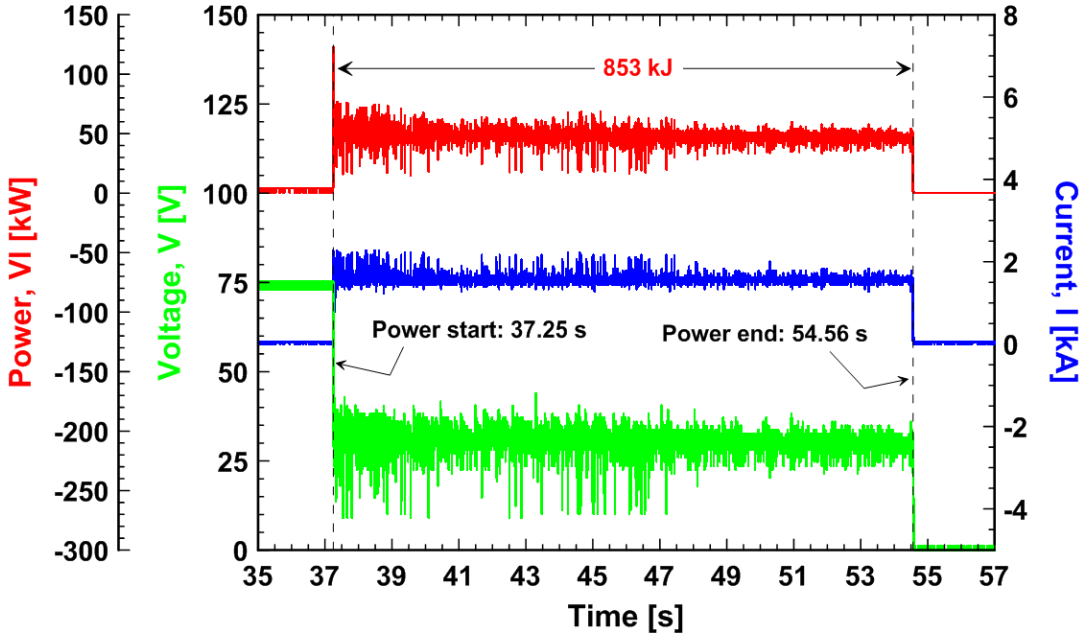

Figure 16. VI Data in Test MM4

The two cell temperatures and the average temperature are plotted vs. time in Fig. 17. The start time for this test was t_1 = 77 s at which time the cell temperature was T_1 = 69.6°C. Power input is terminated 17.3 s later at t' = 94.32 s. During this period the cell temperature rises rapidly from about 70°C to about 530°C due to plasma power generation and electrode power input. When the electrode power is removed the cell temperature decays, first rapidly and then more slowly in a mostly linear trend due to heat loss. At time t_2 = 170 s the final cell temperature is T_2 = 374°C. At this time the uncertainty in cell temperature is about 2.5°C, which is less than a percent of the cell temperature change $T_2 - T_1$ = 304.2°C. The cell enthalpy rise is $\Sigma m_i C_{pi} (T_2 - T_1)$ = 1730.4 kJ. Heat loss by the $\int \dot{Q}_{Loss}$-method, Q_{Loss} = 547.6 kJ. Larger heat losses are predicted owing to the 397°C average cell temperature over the 93 s test duration. The corresponding hydrino reaction energy release and gain as well as the same parameters considering the extreme case of ignoring heat loss completely are:

$Q_{Loss} = 0$:	$E_{Plasma} = 877.3$ kJ;	$\eta = 2.03$
$\int \dot{Q}_{Loss}$-method:	$E_{Plasma} = 1425$ kJ;	$\eta = 2.67$

The relative magnitudes of the various energy quantities in the energy balance are shown in the bar graph of Fig. 18. Note that in test MM4 the heat loss accounts for more than 35% of the plasma energy. All data used in the energy balances are tabulated in Appendix 3.

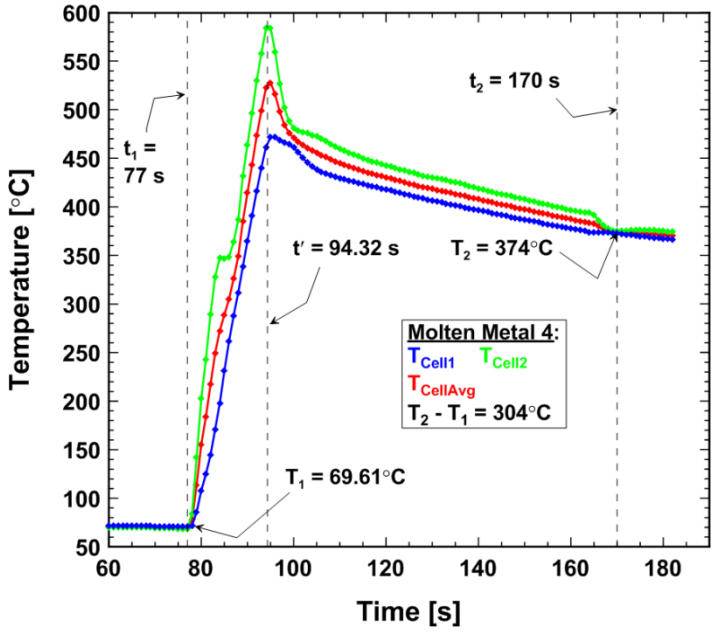

Figure 17. Cell Temperature Variations in Test MM4.

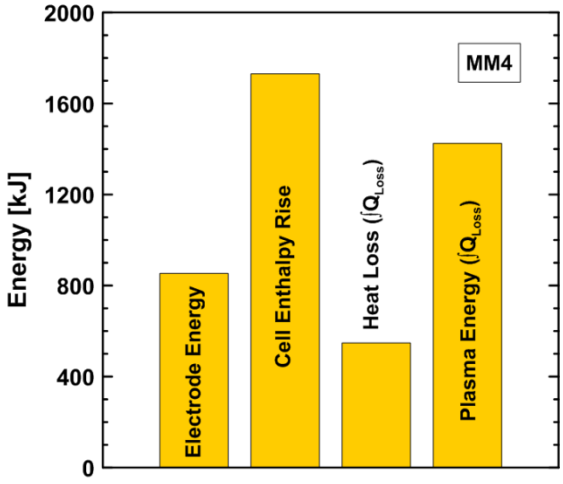

Figure 18. Energy Bar Graph for Test MM4.

References

1. Yovanovich, M.M and K. Jarfarpur Models of Laminar Natural Convection from Vertical and Horizontal Isothermal Cuboids for All Prandtl Numbers and All Rayleigh Numbers Below 10^{11} *ASME Winter Annual Meeting*, New Orleans, LA, Nov. 28-Dec. 5 (1993).
2. Incropera, F.P. and D.P. DeWitt *Fundamentals of Heat and Mass Transfer*, Wiley (1996).

Appendix 1. System Enthalpy Change in Terms of Mass-Weighted Averages

The time rate of change of the system enthalpy is

$$\frac{dH}{dt} = \sum \frac{d}{dt} \int_{m_i} h_i'' dm_i = \sum \int_{m_i} \frac{dh_i''}{dt} dm_i$$

where the subscript i denotes the ith distinct part of the cell, e.g. liquid metal, cell body, cell liner, electrode parts, etc., double primes denote quantities which vary both spatially and temporally, and it is permissible to interchange the operations of integration and differentiation because the mass of each part m_i is fixed. Because the pressure is constant $dh_i'' = C_{pi}'' dT_i''$ so

$$\int_{m_i} \frac{dh_i''}{dt} dm_i = \int_{m_i} C_{pi}'' \frac{dT_i''}{dt} dm_i$$

Introduce the mass-weighted average

$$( )_i' = \frac{\int_{m_i} ( )_i'' dm_i}{\int_{m_i} dm_i}$$

where the single prime denotes variation with time only. And decomposing the specific heat and temperature for the ith part into the mass-weighted average plus the deviation from the average

$$C''_{pi} = \underbrace{C'_{pi}}_{\substack{\text{Mass-weighted average} \\ \text{specific heat for } m_i}} + \underbrace{\delta C''_{pi}}_{\substack{\text{Local specific heat} \\ \text{deviation from the average}}}, \qquad T_i'' = \underbrace{T'_i}_{\substack{\text{Mass-weighted average} \\ \text{temperature for } m_i}} + \underbrace{\delta T''_i}_{\substack{\text{Local temperature} \\ \text{deviation from the average}}}$$

results in

$$\int_{m_i} C''_{pi} \frac{dT''_i}{dt} dm_i = \int_{m_i} \left(C'_{pi} + \delta C''_{pi}\right)\left(\frac{dT'_i}{dt} + \frac{d(\delta T''_i)}{dt}\right) dm_i$$

$$= \int_{m_i} C'_{pi} \frac{dT'_i}{dt} dm_i + \int_{m_i} C'_{pi} \frac{d(\delta T''_i)}{dt} dm_i + \int_{m_i} \delta C''_{pi} \frac{dT'_i}{dt} dm_i + \int_{m_i} \delta C''_{pi} \frac{d(\delta T''_i)}{dt} dm_i$$

Since the mass-averages C'_{pi} and T'_i are independent of position

$$\int_{m_i} C''_{pi} \frac{dT''_i}{dt} dm_i = m_i C'_{pi} \frac{dT'_i}{dt} + C'_{pi} \frac{d}{dt} \int_{m_i} \delta T''_i dm_i + \frac{dT'_i}{dt} \int_{m_i} \delta C''_{pi} dm_i + \int_{m_i} \delta C''_{pi} \frac{d(\delta T''_i)}{dt} dm_i \quad \text{(A1.1)}$$

The second and third terms on the right of (A1.1) are zero because the averages of the deviations vanish and the last term on the right is small because the deviation $\delta C''_{pi}$ is small and because of cancellation owing to changing sign of the integrand. Then, the time rate of system enthalpy change is given in terms of the mass-weighted mean specific heats and time derivatives of the mass-weighted mean temperature for the various cell component parts:

$$\frac{dH}{dt} = \sum m_i C'_{pi} \frac{dT'_i}{dt}$$

The time integral over the test run interval $t_1 < t < t_2$

$$\int_{t_1}^{t_2} C'_{pi} \frac{dT'_i}{dt} dt = \int_{T_1}^{T_2} C'_{pi} dT'_i = C_{pi}(T_2 - T_1)$$

where

$$C_{pi} = \frac{\int_{T_1}^{T_2} C'_{pi} dT'_i}{\int_{T_1}^{T_2} dT'_i}$$

is the specific heat of component part i averaged over temperatures from the initial temperature T_1 to the final temperature T_2. Here, isothermality ($T_i = T_2$) of the various cell parts at time t_2 has been assumed.

Appendix 2. Estimate of Temperature Drop Through Cell Liner and Wall

Thermal transfer from the liquid metal inside the cell to the surroundings is shown schematically in Fig. 2. Ignoring transient effects and convective resistance at the liquid/liner interface the rate of conduction heat transfer through the cell liner/cell wall is

$$q_{Cond} = k_{Liner}\frac{(T_{LM} - T')}{\delta_{Liner}} = k_W\frac{(T' - T_S)}{\delta_W} = \frac{\frac{k_{Liner}}{\delta_{Liner}}(T_{LM} - T_S)}{1 + \frac{k_{Liner}}{k_W}\frac{\delta_W}{\delta_{Liner}}}$$

where k denotes thermal conductivity. The heat flux from the cell surface is $q_{Conv} + q_{Rad} = q_{Cond}$ with the radiative flux

$$q_{Rad} = \sigma\varepsilon(T_S^4 - T_\infty^4)$$

where ε is emissivity of the cell wall. The free convection flux is

$$q_{Conv} = h(T_S - T_\infty), \quad h = \frac{Nu_L k}{L}$$

where h is the convection coefficient, L is the cell characteristic dimension for convection, the Nusselt number is

$$Nu_L = Nu_L(Ra_L, Pr)$$

$$Ra_L = \frac{g\beta(T_S - T_\infty)L^3}{\nu\alpha}, \quad \text{Rayliegh number}$$

$$Pr = \frac{\nu}{\alpha}, \quad \text{Prandtl number}$$

and the thermal properties for air (k, β, ν, α) are evaluated at the film temperature $T_{film} = (T_S + T_\infty)/2$. According to Yovanovich and Jarfarpur [1], for the cubical cells with side length W

$$L = \sqrt{\text{Cube Surface Area}} = \sqrt{A} = \sqrt{6W^2}$$

and the Nusselt number is

$$Nu_{\sqrt{A}} = Nu_{\sqrt{A}}^{\infty} + F(Pr)G_{\sqrt{A}}Ra_{\sqrt{A}}^{1/4}$$

where the diffusive limit $Nu_{\sqrt{A}}^{\infty} = 3.39$ and the body-gravity function $G_{\sqrt{A}} = 0.984$ for cubes, and the Prandtl number function is

$$F(Pr) = \frac{0.670}{\left[1 + (0.5/Pr)^{9/16}\right]^{4/9}}$$

For the spherical cell the characteristic dimension is the diameter D and the Nusselt number is given by Incropera and DeWitt [2]:

$$Nu_D = 2 + \frac{0.589Ra_D^{1/4}}{\left[1 + (0.469/Pr)^{9/16}\right]^{4/9}}$$

For example, for a cubical 347 stainless steel cell with stably oxidized surface (ε = 0.88), 1/4 inch thick wall and 3 mm tungsten liner, a liquid metal temperature of 500°C results in a surface temperature of 493.1°C and the fluxes q_{Conv} = 3622 W/m^2 and q_{Rad} = 16,802 W/m^2.

Appendix 3. Energy Balance Data Tables

Energy Balance Data: MM1

Test MM1

Times	
t_1 [s]	77
t' [s]	99.4
t_2 [s]	129
(t' - t_1) [s]	22.4
(t_2 - t_1) [s]	52

Cell temperatures	
T_{init1} [°C]	86.65
T_{init2} [°C]	88.78
T_{final1} [°C]	480.28
T_{final2} [°C]	472.75
T_1 [°C]	87.72
T_2 [°C]	476.52
(T_2 - T_1) [°C]	388.80

Energy and power	Energy [kJ]	Power [kW]
Cell enthalpy rise, $(\Sigma m_i C_{pi})(T_2 - T_1)$	2042.54	
Electrode input, E_{Elect}	774.8	34.59
Energy loss ($\int Q_{Loss}(T)$), Q_{Loss}	425.6	8.18
Plasma energy generation (Q_{Loss} = 0), E_{Plasma}	1267.74	56.60
Plasma energy generation ($\int Q_{Loss}(T)$), E_{plasma}	1693.34	75.60

Gain	
Gain (Q_{Loss} = 0), (E_{Plasma} + E_{Elect})/E_{Elect}	2.64
Gain ($\int Q_{Loss}(T)$), (E_{Plasma} + E_{Elect})/E_{Elect}	3.19

Cell component thermal capacities

	m_i [kg]	C_{pi} [kJ/kg-K]	$m_i C_{pi}$ [kJ/K]
Gallium	0	0.383	0
Galinstan	3.4	0.3	1.02
Stainless cell	6.2	0.502	3.1124
Stainless electrode	1.26	0.502	0.63252
Tungsten electrode	1.52	0.1339	0.203528
Copper electrode	0.369	0.39	0.14391
BN electrode	0.166	0.85	0.1411
Tungsten liner	0	0.1339	0
Tantalum liner	0	0.14	0
Reservoir	0	0.794	0
Totals	12.915		5.253458

Energy Balance Data: MM2

Test MM2

Times	
t_1 [s]	24
t' [s]	25.27
t_2 [s]	50
(t' - t_1) [s]	1.27
(t_2 - t_1) [s]	26

Cell temperatures	
T_{init1} [°C]	56.41
T_{init2} [°C]	56.21
T_{final1} [°C]	137.10
T_{final2} [°C]	139.16
T_1 [°C]	56.31
T_2 [°C]	138.13
(T_2 - T_1) [°C]	81.82

Energy and power	Energy [kJ]	Power [kW]
Cell enthalpy rise, $(\Sigma m_i C_{pi})(T_2 - T_1)$	455.85	
Electrode input, E_{Elect}	212.9	167.64
Energy loss ($\int Q_{Loss}(T)$), Q_{Loss}	29.9	1.15
Plasma energy generation ($Q_{Loss} = 0$), E_{Plasma}	242.95	191.30
Plasma energy generation ($\int Q_{Loss}(T)$), E_{plasma}	272.85	214.84

Gain	
Gain ($Q_{Loss} = 0$), $(E_{Plasma} + E_{Elect})/E_{Elect}$	2.14
Gain ($\int Q_{Loss}(T)$), $(E_{Plasma} + E_{Elect})/E_{Elect}$	2.28

Cell component thermal capacities	m_i [kg]	C_{pi} [kJ/kg-K]	$m_i C_{pi}$ [kJ/K]
Gallium	2.5	0.383	0.9575
Galinstan	0	0.3	0
Stainless cell	6.4	0.502	3.2128
Stainless electrode	1.26	0.502	0.63252
Tungsten electrode	1.52	0.1339	0.203528
Copper electrode	0.369	0.39	0.14391
BN electrode	0.166	0.85	0.1411
Tungsten liner	0	0.1339	0
Tantalum liner	2	0.14	0.28
Reservoir	0	0.794	0
Totals	14.215		5.571358

Energy Balance Data: MM3

Test MM3

Times	
t_1 [s]	111
t' [s]	122.99
t_2 [s]	155
(t' - t_1) [s]	11.99
(t_2 - t_1) [s]	44

Cell temperatures	
T_{init1} [°C]	82.91
T_{init2} [°C]	84.00
T_{final1} [°C]	321.44
T_{final2} [°C]	331.35
T_1 [°C]	83.46
T_2 [°C]	326.40
(T_2 - T_1) [°C]	242.94

Energy and power	Energy [kJ]	Power [kW]
Cell enthalpy rise, $(\Sigma m_i C_{pi})(T_2 - T_1)$	1382.16	
Electrode input, E_{Elect}	625.7	52.19
Energy loss ($\int Q_{Loss}(T)$), Q_{Loss}	174	3.95
Plasma energy generation ($Q_{Loss} = 0$), E_{Plasma}	756.46	63.09
Plasma energy generation ($\int Q_{Loss}(T)$), E_{plasma}	930.46	77.60

Gain	
Gain ($Q_{Loss} = 0$), $(E_{Plasma} + E_{Elect})/E_{Elect}$	2.21
Gain ($\int Q_{Loss}(T)$), $(E_{Plasma} + E_{Elect})/E_{Elect}$	2.49

Cell component thermal capacities	m_i [kg]	C_{pi} [kJ/kg-K]	$m_i C_{pi}$ [kJ/K]
Gallium	2.7	0.383	1.0341
Galinstan	0	0.3	0
Stainless cell	6.4	0.502	3.2128
Stainless electrode	1.26	0.502	0.63252
Tungsten electrode	1.52	0.1339	0.203528
Copper electrode	0.369	0.39	0.14391
BN electrode	0.166	0.85	0.1411
Tungsten liner	2.4	0.1339	0.32136
Tantalum liner	0	0.14	0
Reservoir	0	0.794	0
Totals	14.815		5.689318

Energy Balance Data: MM4

Test MM4

Times	
t_1 [s]	77
t' [s]	94.3
t_2 [s]	170
(t' - t_1) [s]	17.3
(t_2 - t_1) [s]	93

Cell temperatures	
T_{init1} [°C]	70.55
T_{init2} [°C]	68.66
T_{final1} [°C]	372.51
T_{final2} [°C]	375.01
T_1 [°C]	69.61
T_2 [°C]	373.76
(T_2 - T_1) [°C]	304.16

Energy and power	Energy [kJ]	Power [kW]
Cell enthalpy rise, $(\Sigma m_i C_{pi})(T_2 - T_1)$	1730.43	
Electrode input, E_{Elect}	853.1	49.31
Energy loss ($\int Q_{Loss}(T)$), Q_{Loss}	547.6	5.89
Plasma energy generation ($Q_{Loss} = 0$), E_{Plasma}	877.33	50.71
Plasma energy generation ($\int Q_{Loss}(T)$), E_{plasma}	1424.93	82.37

Gain	
Gain ($Q_{Loss} = 0$), ($E_{Plasma} + E_{Elect}$)/E_{Elect}	2.03
Gain ($\int Q_{Loss}(T)$), ($E_{Plasma} + E_{Elect}$)/E_{Elect}	2.67

Cell component thermal capacities	m_i [kg]	C_{pi} [kJ/kg-K]	$m_i C_{pi}$ [kJ/K]
Gallium	2.7	0.383	1.0341
Galinstan	0	0.3	0
Stainless cell	6.4	0.502	3.2128
Stainless electrode	1.26	0.502	0.63252
Tungsten electrode	1.52	0.1339	0.203528
Copper electrode	0.369	0.39	0.14391
BN electrode	0.166	0.85	0.1411
Tungsten liner	2.4	0.1339	0.32136
Tantalum liner	0	0.14	0
Reservoir	0	0.794	0
Totals	14.815		5.689318